Lateral Stability of Gliding Parachutes

Peter Crimi*
Textron Defense Systems, Wilmington, Massachusetts 01887

The lateral stability of a gliding parachute or other lifting surface with a suspended payload is analyzed to determine the relationship of aerodynamic and inertial parameters to stability characteristics. The system is represented by a rigid wing with a suspended payload in a steady glide. As with conventional fixed-wing aircraft, the lateral response is characterized by an oscillatory response mode and a spiral divergence. The stability boundary for spiral divergence can be prescribed analytically. Calculations show that there is a minimum effective anhedral angle required for absolute stability. Increasing suspension line length is stabilizing for spiral divergence, whereas increasing the glide slope is stabilizing for both spiral divergence and oscillatory response.

Nomenclature

b	= wingspan
C_{DL}	= payload drag coefficient
C_{Dw}	= wing drag coefficient
C_l^*	= rolling moment coefficient; see Eq. (2)
C_l	= coefficient of rolling moment about wing axis
C_L	= wing lift coefficient
C_m	= wing pitching moment coefficient
C_n^*	= yawing moment coefficient; see Eq. (3)
C_n	= coefficient of yawing moment about wing axis
C_Y	= side force coefficient; see Eq. (1)
F_Y	= side force
I_{xx},I_{zz},I_{xz}	= moments and product of inertia
L	= rolling moment
m	= total mass
N	= yawing moment
p	= role rate
r	= yaw rate
S	= wing area
s_l	= height of wing above mass center
u,v	= components of velocity in X,Y directions
V	= magnitude of resultant velocity
W	= total weight
X,Y,Z	= axes defined in Fig. 1, with origin at mass center
α	= angle of attack
β	= sideslip angle
Γ	= wing dihedral angle
γ	= flight-path angle; glide slope = $-\tan\gamma$
δ	= distance of wing aft of mass center
λ	= characteristic value
μ	= mass ratio, $\mu = m/(\rho Sb)$
ρ	= air density
τ	= dimensionless time, $\tau = (\rho SV/m)t$
ϕ,ψ	= roll and yaw angles, respectively

Subscripts

p	= derivative with respect to $pb/(2V)$
r	= derivative with respect to $rb/(2V)$

Introduction

ALTHOUGH the lateral stability characteristics of conventional fixed-wing aircraft have been extensively studied,[1,2] gliding parachutes such as parafoils and paragliders have not received this attention. Some understanding of the factors governing lateral stability has been derived empirically from testing[3,4] and numerical simulation,[5,6] however. This analysis was directed to quantifying the relationships of aerodynamic and inertial parameters to gliding parachute lateral stability.

The system analyzed consists of a rigid wing with a suspended payload in a steady glide, as shown in Fig. 1. As far as possible, the formulations used parallel directly those used for conventional aircraft[1] to allow a comparison of results where appropriate. Since the effects of suspending the payload on the aerodynamic loading play a large role in defining the lateral stability, the aerodynamic loading is first formulated in what follows. The characteristic equation is then derived, and results of calculations are presented for representative configurations.

Aerodynamic Loading

The response and loading are referred to axes X,Y,Z, with origin at the mass center, as defined in Fig. 1. Note that X and Z are wind-fixed and that Y is body-fixed. The variables governing lateral response are the roll angle ϕ, the role rate $p = \dot{\phi}$, the yaw angle ψ, the yaw rate $r = \dot{\psi}$, and the slideslip angle β. The relevant aerodynamic loads are side force F_Y, rolling moment L, and yawing moment N. With the composite mass center a distance s_l below and δ forward of the wing mass center, the sideslip angle at the wing is $\beta + s_l p/V - \delta r/V$. As a result, the loads, in coefficient form, are as follows:

$$C_Y = \frac{2F_Y}{(\rho V^2 S)} = C_{Y\beta}\left(\beta + \frac{s_l p}{V} - \frac{\delta r}{V}\right) \tag{1}$$

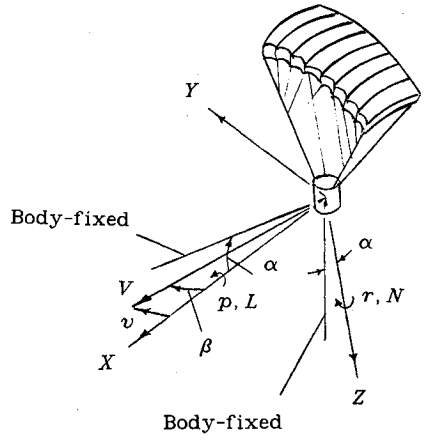

Fig. 1 Coordinate system.

Received Dec. 23, 1988; revision received May 23, 1989.

*Principal Scientist. Member AIAA.

$$C_l^* = \frac{2L}{(\rho V^2 Sb)} = C_{lp}\left(\frac{pb}{2V}\right) + \left(C_{l\beta} + \frac{s_l}{b}C_{Y\beta}\right)\left(\beta + \frac{s_l p}{V} - \frac{\delta r}{V}\right) + C_{lr}\left(\frac{rb}{2V}\right) \quad (2)$$

$$C_n^* = \frac{2N}{(\rho V^2 Sb)} = C_{np}\left(\frac{pb}{2V}\right) + \left(C_{n\beta} - \frac{\delta}{b}C_{Y\beta}\right)\left(\beta + \frac{s_l p}{V} - \frac{\delta r}{V}\right) + C_{nr}\left(\frac{rb}{2V}\right) \quad (3)$$

In Eqs. (2) and (3), C_l^* and C_n^* are coefficients of the roll and yaw moments, respectively, about the composite mass center, while C_l and C_n are coefficients of the roll and yaw moments, respectively, about the wing mass center.

It was found most convenient to define stability boundaries with the yaw static-stability coefficient $C_{n\beta}$ as a dependent variable, as was done in Ref. 1. The other coefficients in Eqs. (1–3) can be expressed, to varying degrees of accuracy, in terms of wing and flight parameters. The relations used, taken from Refs. 1 and 2, are as follows:

$$C_{Y\beta} = -\Gamma^2 \frac{dC_L}{d\alpha}$$

$$C_{l\beta} = -\frac{\Gamma}{4}\frac{dC_L}{d\alpha}$$

$$C_{lp} = -\left(\frac{dC_L}{d\alpha} + C_{Dw}\right)\Big/ 8$$

$$C_{lr} = C_L/3$$

$$C_{np} = -\left(C_L - \frac{dC_{Dw}}{d\alpha}\right)\Big/ 8$$

$$C_{nr} = -C_{Dw}/4$$

In the absence of test data, an appropriate value for Γ in the preceding expressions is somewhat uncertain for canopies that typically form a circular arc, sometimes with vertical skirts at the ends for lateral stability. The anhedral angle of an equivalent wing formed by the chords of the arc drawn from the apex to the wing tips was used in Ref. 7.

The distance of the wing mass center aft of the composite mass center is determined by the longitudinal trim of the parachute. Summing moments about the wing mass center, it is found that

$$\frac{\delta}{b} = \frac{[C_m - C_{DL}(s_l/b)]}{C_L} - \frac{s_l}{b}\tan\gamma$$

where C_m is the wing pitching moment coefficient. Note that the static stability in yaw, which will be seen to play a major role in determining dynamic stability, derives from the term $C_{n\beta} - (\delta/b)C_{Y\beta}$ in Eq. (3) and that δ/b, in turn, is a strong function of both s_l/b and the glide slope $-\tan\gamma$.

Derivation of the Characteristic Equation

Using the coordinates defined in Fig. 1, the equations governing the lateral response are as follows:

$$v\frac{\partial F_Y}{\partial v} + p\frac{\partial F_Y}{\partial p} + r\frac{\partial F_Y}{\partial r} + W(\phi\cos\gamma + \psi\sin\gamma) = m(\dot{v} + ru) \quad (4)$$

$$v\frac{\partial L}{\partial v} + p\frac{\partial L}{\partial p} + r\frac{\partial L}{\partial r} = I_{xx}\dot{p} + I_{xz}\dot{r} \quad (5)$$

$$v\frac{\partial N}{\partial v} + p\frac{\partial N}{\partial p} + r\frac{\partial N}{\partial r} = I_{xz}\dot{p} + I_{zz}\dot{r} \quad (6)$$

The total mass m includes the apparent mass of the canopy, which simulation results[5] indicate should be about half the mass of the displaced air for a ram air parachute. In a steady glide, $W\cos\gamma = \frac{1}{2}\rho V^2 S C_L$. Also, $\beta \approx v/V$, $p = \dot{\phi}$, $r = \dot{\psi}$, and $u \approx V$. Further, the following quantities are defined:

$$\tau = \frac{\rho SV}{m}t, \quad \mu = \frac{m}{\rho Sb}, \quad h_{xx} = \frac{4I_{xx}}{mb^2}, \quad h_{zz} = \frac{4I_{zz}}{mb^2}$$

$$h_{xz} = \frac{4I_{xz}}{mb^2}, \quad y_s = \frac{C_{Y\beta}}{\mu}\frac{s_l}{b}, \quad y_\delta = \frac{C_{Y\beta}}{\mu}\frac{\delta}{b} + 2$$

$$l_\beta = C_{l\beta} + \frac{s_l}{b}C_{Y\beta}, \quad n_\beta = C_{n\beta} - \frac{\delta}{b}C_{Y\beta}, \quad l_p = C_{lp} + 2\frac{s_l}{b}l_\beta$$

$$n_p = C_{np} + 2\frac{s_l}{b}n_\beta, \quad l_r = C_{lr} - 2\frac{\delta}{b}l_\beta, \quad n_r = C_{nr} - 2\frac{\delta}{b}n_\beta$$

Using these relations and substituting from Eqs. (1), (2), and (3) for F_Y, L, and N, respectively, the equations of motion can be written as follows:

$$C_{Y\beta}\beta - 2\frac{d\beta}{d\tau} + C_L\phi + y_s\frac{d\phi}{d\tau} + C_L\tan\gamma\psi - y_\delta\frac{d\psi}{d\tau} = 0 \quad (7)$$

$$2\mu l_\beta\beta + l_p\frac{d\phi}{d\tau} - h_{xx}\frac{d^2\phi}{d\tau^2} + l_r\frac{d\psi}{d\tau} - h_{xz}\frac{d^2\psi}{d\tau^2} = 0 \quad (8)$$

$$2\mu n_\beta\beta + n_p\frac{d\phi}{d\tau} - h_{xz}\frac{d^2\phi}{d\tau^2} + n_r\frac{d\psi}{d\tau} - h_{zz}\frac{d^2\psi}{d\tau^2} = 0 \quad (9)$$

If $\beta = \bar{\beta}e^{\lambda\tau}$, $\phi = \bar{\phi}e^{\lambda\tau}$, and $\psi = \bar{\psi}e^{\lambda\tau}$ are substituted in these equations, the characteristic equation is found to be

$$A\lambda^4 + B\lambda^3 + C\lambda^2 + D\lambda + E = 0$$

where

$$A = h_{xx}h_{zz} - h_{xz}^2$$

$$B = -\frac{C_{Y\beta}}{2}A - h_{xx}n_r - h_{zz}l_p + h_{xz}(l_r + n_p)$$

$$C = \frac{C_{Y\beta}}{2}[h_{xx}n_r + h_{zz}l_p - h_{xz}(l_r + n_p)] - n_p l_r + l_p n_r - \mu l_\beta(y_s h_{zz} + y_\delta h_{xz}) + \mu n_\beta(y_s h_{xz} + y_\delta h_{xx})$$

$$D = \frac{C_{Y\beta}}{2}(n_p l_r - l_p n_r) + \mu l_\beta(y_s n_r + y_\delta n_p - h_{zz}C_L + h_{xz}C_L\tan\gamma) - \mu n_\beta(y_s l_r + y_\delta l_p - h_{xz}C_L + h_{xx}C_L\tan\gamma)$$

$$E = \mu C_L[l_\beta(n_r - n_p\tan\gamma) - n_\beta(l_r - l_p\tan\gamma)]$$

Effects of Parameters on Stability

The characteristic equation generally yields two real roots and a pair of complex conjugate roots. As is the case with conventional airplanes, one of the real roots has a large negative value and is not of concern with regard to stability. The other three roots may or may not cause divergent lateral response. For a given set of geometric, inertial, and aerodynamic parameters, the response was typically found to be characterized by a range of values for $C_{n\beta}$ within which the response is positively damped. If $C_{n\beta}$ exceeds an upper bound (note that positive $C_{n\beta}$ implies static stability in yaw), the characteristic equation has a positive real root that results in what is termed spiral divergence.[2] If $C_{n\beta}$ is reduced below a lower bound, a complex pair of roots with a positive real part is found, resulting in an oscillatory instability.

The location of the spiral divergence boundary can be examined analytically since neutral stability results when the constant E in the characteristic equation vanishes. By setting

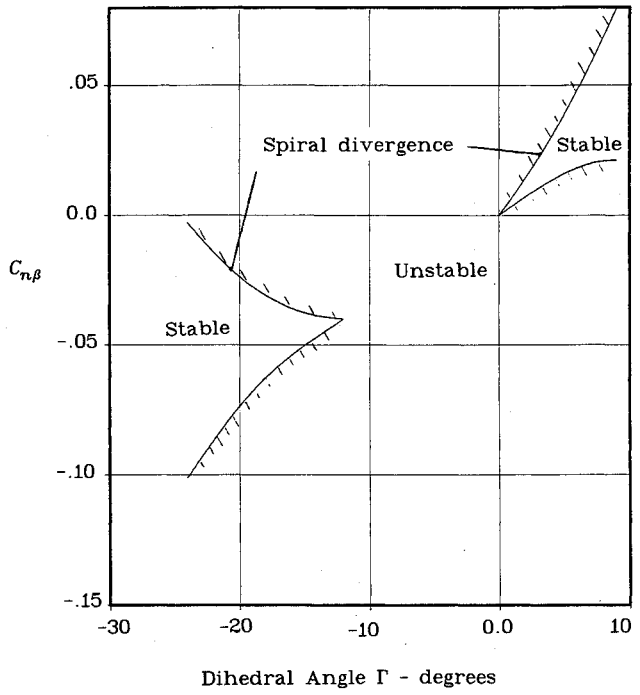

Fig. 2 Effect of dihedral on stability; $-\tan\gamma = 1/3$, $s_l/b = 1.2$.

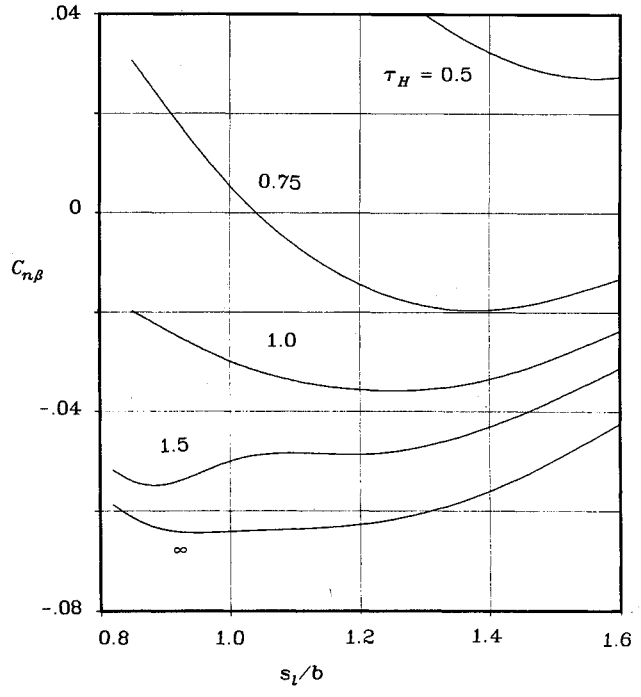

Fig. 3 Effect of suspension line length on oscillatory response; $-\tan\gamma = 1/3$, $\Gamma = -18$ deg.

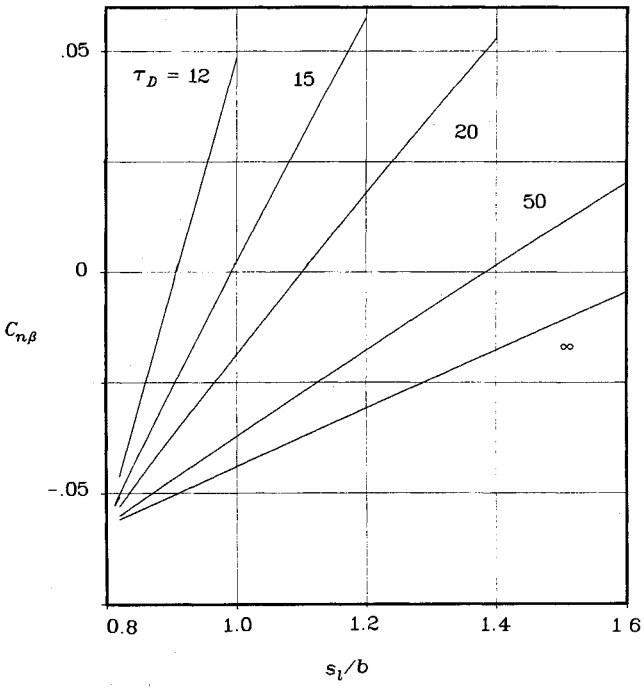

Fig. 4 Effect of suspension line length on spiral divergence; $-\tan\gamma = 1/3$, $\Gamma = -18$ deg.

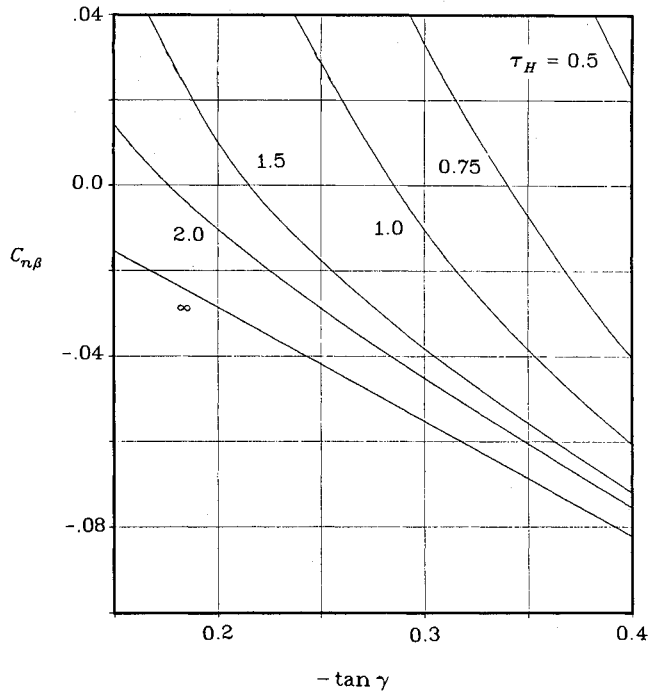

Fig. 5 Effect of glide slope on oscillatory response; $s_l/b = 1$, $\Gamma = -18$ deg.

the expression for E to zero, the following relation for the value of $C_{n\beta}$ to cause spiral divergence is found:

$$C_{n\beta} = \frac{(C_{l\beta} + (s_l/b)C_{Y\beta})(C_{nr} - C_{np}\tan\gamma)}{(C_{lr} - C_{lp}\tan\gamma)} + \frac{\delta}{b}C_{Y\beta}$$

It is evident from this expression that the stability boundary is a strong function of s_l, the glide slope $-\tan\gamma$, and the dihedral angle Γ. The lift coefficient C_L has considerable effect, too, since C_{lr} is proportional to C_L. Note that the mass ratio μ, which is proportional to the wing loading, has no effect on the spiral divergence boundary, nor do the moments of inertia.

Roots of the characteristic equation were calculated using the Descartes-Euler solution for a quartic, varying s_l/b, the dihedral angle, and the glide slope. Nominal values were assigned to those quantities that have little or no effect on stability boundaries, as follows:

$$\mu = 20, \quad h_{xx} = 0.27, \quad h_{zz} = 0.038, \quad h_{xz} = -0.1\frac{s_l}{b}\frac{\delta}{b}$$

$$C_L = 0.6726, \quad C_{L\alpha} = 2.86, \quad \frac{dC_D}{d\alpha} = 0.618,$$

$$C_{DL} = 0.0315, \quad C_m = -0.0164$$

The effect of dihedral angle on stability is shown in Fig. 2 for $s_l/b = 1.2$ and a glide slope of 1/3. For Γ between -12 deg and zero, the static stability derived by suspending the payload is not sufficient to overcome the destabilizing effect of anhedral, and so the vehicle is unstable, regardless of the value of $C_{n\beta}$. As Γ decreases below -12 deg or increases above zero, stable flight results with $C_{n\beta}$ values below the spiral divergence boundary and above the oscillatory stability boundary. Note that, for typical parafoil configurations with large effective anhedral, the canopy itself must have negative $C_{n\beta}$, i.e., it must be statistically unstable in yaw, to preclude spiral divergence, because of the static yaw stability afforded by the mass center offset δ.

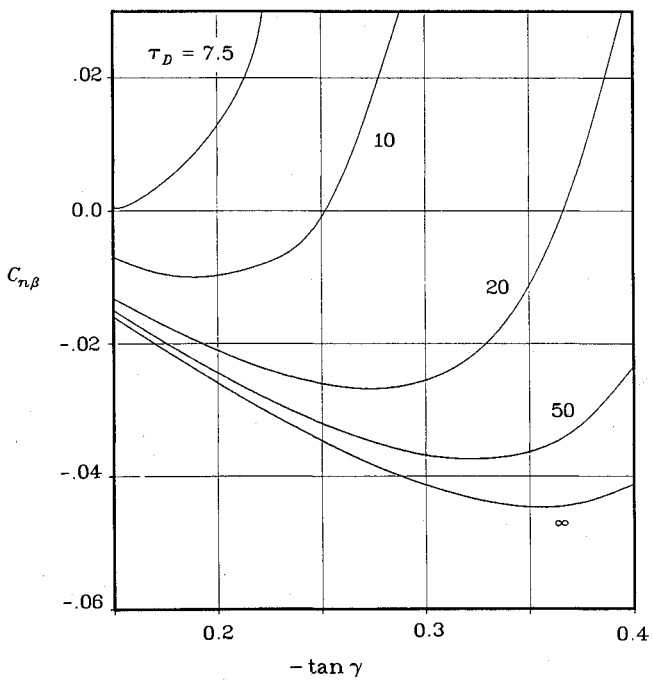

Fig. 6 Effect of glide slope on spiral divergence; $s_l/b = 1$, $\Gamma = -18$ deg.

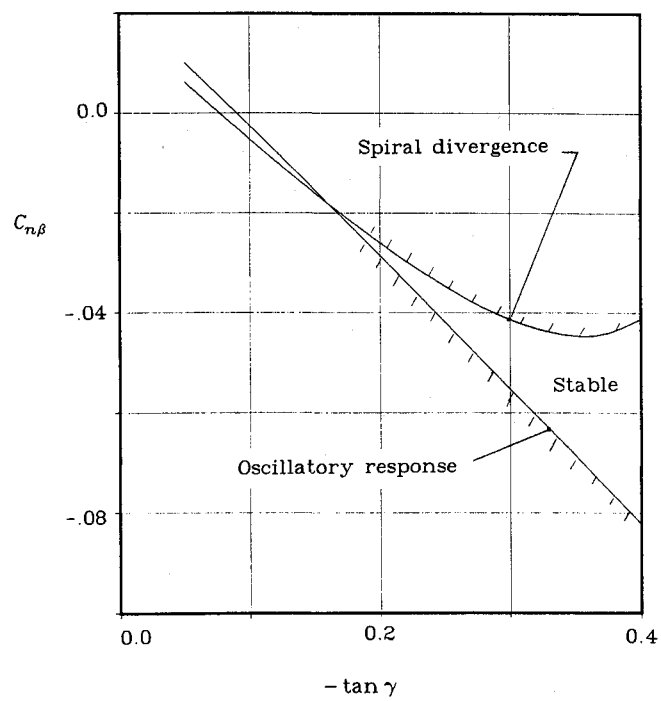

Fig. 7 Effect of glide slope on stability boundaries; $s_l/b = 1$, $\Gamma = -18$ deg.

The effect of suspension line length on lateral stability is shown in Figs. 3 and 4, for a glide slope of 1/3 and a dihedral angle of -18 deg. The oscillatory stability boundary and lines of constant dimensionless time τ_H to damp to half-amplitude are plotted in Fig. 3, and the spiral divergence boundary and lines of constant time to double amplitude τ_D are plotted in Fig. 4, against s_l/b. Note that s_l is the distance of the wing mass center above the composite mass center and so includes the distance from the composite mass center to the suspension line attachment to the payload. The stability of the oscillatory mode is seen to be relatively insensitive to s_l/b, but increasing s_l/b for a given value of $C_{n\beta}$ markedly improves the stability of the spiral divergence mode. At s_l/b of 0.81, the boundaries of spiral divergence and oscillatory instability cross. As a result, the character of the solution changes for s_l/b less than 0.81. The system is then unstable, regardless of the value of $C_{n\beta}$, the reduced pendular stability in roll being insufficient to overcome the effects of anhedral.

The effect of glide slope is shown in Figs. 5 and 6 for $s_l/b = 1$ and a dihedral angle of -18 deg. Increasing the glide slope (i.e., decreasing the ratio of lift to drag) increases stability for both oscillatory response, Fig. 5, and spiral divergence, Fig. 6. Note, from Fig. 7, where the stability boundaries are replotted on the same graph, that as the glide slope is reduced, the range of values of $C_{n\beta}$ within which the system is stable in both modes becomes smaller. If the glide slope is less than about 0.15, spiral divergence is unavoidable if the oscillatory mode is positively damped.

Conclusions

The lateral stability characteristics of gliding parachutes are, in some respects, similar to those of conventional fixed-wing aircraft. Both systems exhibit an oscillatory mode of response and a tendency toward spiral divergence. Also, inertial characteristics, including apparent mass effects and wing loading, have little or no effect on stability boundaries in both cases. The static stability in roll afforded by suspending the payload distinguishes gliding parachutes, however, with the following relations observed from the calculation results:

1) For a given suspension line length, a minimum effective anhedral angle is required for stability. As with airplanes, positive dihedral also produces a region of absolutely stable response.

2) Increasing suspension line length is stabilizing for spiral divergence but has little effect on oscillatory response. There is a minimum suspension line length below which the system is unstable, regardless of the static stability in yaw.

3) Decreasing the glide slope is destabilizing for both oscillatory response and spiral divergence. For a very small glide slope, spiral divergence is unavoidable if the oscillatory response is positively damped.

These conclusions may be modified to some exent by the effects of canopy flexibility, which were neglected in the analysis.

References

[1]Zimmerman, C., "An Analysis of Lateral Stability in Power-Off Flight With Charts for Use in Design," NACA Rept. 589, 1937.

[2]Perkins, C., and Hage, R., *Airplane Performance, Stability and Control*, Wiley, New York, 1957, pp. 419–433.

[3]Puskas, E., "Ram Air Parachute Design Considerations and Applications," AIAA Paper 84-0826, April 1984.

[4]Mayer, R. T., "Controlled Terminal Descent and Recovery of Large Aerospace Components," AIAA Paper 86-2467, Oct. 1986.

[5]Goodrick, T., "Simulation Studies of the Flight Dynamics of Gliding Parachute Systems," AIAA Paper 79-0417, Oct. 1979.

[6]Goodrick, T., "Scale Effects on Performance of Ram Air Wings," AIAA Paper 84-0783, April 1984.

[7]Lingard, S., "The Aerodynamics of Gliding Parachutes," AIAA Paper 86-0783, Oct. 1986.